



Ultrastable two-dimensional fluorescent conjugated microporous polymers containing pyrene and fluorene units for metal ion sensing and energy storage

Mohamed Gamal Mohamed^{a,b,*}, Huan-Yu Hu^a, Manivannan Madhu^c, Maha Mohamed Samy^{a,b}, Islam M.A. Mekhemer^{b,d}, Wei-Lung Tseng^c, Ho-Hsiu Chou^d, Shiao-Wei Kuo^{a,e,*}

^a Department of Materials and Optoelectronic Science, College of Semiconductor and Advanced Technology Research, Center of Crystal Research, National Sun Yat-Sen University, Kaohsiung 804, Taiwan

^b Chemistry Department, Faculty of Science, Assiut University, Assiut 71515, Egypt

^c Department of Chemistry, National Sun Yat-sen University, Kaohsiung 804, Taiwan

^d Department of Chemical Engineering, National Tsing Hua University, Hsinchu 30013, Taiwan

^e Department of Medicinal and Applied Chemistry, Kaohsiung Medical University, Kaohsiung 807, Taiwan

ARTICLE INFO

Keywords:

Conjugated microporous polymers
Coupling reaction
Metal ion sensing
Electrochemical performance

ABSTRACT

This study aims to synthesize three conjugated microporous polymers (CMPs) [Py-F CMP, TPE-F CMP, and TBN-F CMP] via the Suzuki coupling reaction of 9,9-dihexylfluorene-2,7-diboronic acid [F-B(OH)₂] with three brominated derivatives, pyrene (Py), tetraphenylethylene (TPE), and tetrabenzonaphthalene (TBN). The functional groups and chemical structures of the three synthesized CMPs were confirmed using FTIR and solid-state NMR analyses. Thermogravimetric analysis (TGA) revealed that TBN-F CMP has the most outstanding $T_{d10} = 418$ °C and char yield = 63.3 wt% compared to the other two samples. The BET surface area and average pore size of TBN-F CMP were measured to be 200 m² g⁻¹ and ca. 1.8 nm, respectively. Furthermore, with excellent photoluminescence (PL) properties, all three new CMPs were well characterized using a spectrophotometer, and the fluorescence emission spectra were clearly drawn. As a result, we found that Py-F CMP can detect Pb²⁺ ions specifically and selectively compared to the other two CMPs. The sensitivity of Pb²⁺ was calculated and fitted with linear coefficients ($R_2 = 0.9752$) to determine the Pb²⁺ ion concentration over the ranges of 0.1–2.0 μM, and the detection limit was estimated to be 0.01 μM. Finally, with outstanding capacitance and stability of up to 195 F g⁻¹ and 90% over 2000 cycles, TBN-F-based CMP has been successfully applied to electrochemical measurements.

1. Introduction

Energy is the most essential requirement for the life and advancement of human civilization. In such situations, a serious scarcity of conventional fossil fuels is seen these days, which might be due to several reasons, such as rapid growth of the economy, society, and the increasing rate of environmental contamination [1–10]. Although there are many alternative methods to eliminate these demands, such as renewable sources of energy, such as solar power, wind energy, and geothermal energy, it is still not a smart idea as they not only focus on providing electricity but also rise their raw material [11–13]. Additionally, the increase in global warming demonstrates that fossil fuels

also affect ecosystems because of continued carbon dioxide (CO₂) emissions [14]. Therefore, considering these impacts and addressing the current situation, it is crucial to develop materials that can effectively handle the energy-storage process. Recently, there have been a few existing materials that have become trends with high storage densities, such as lithium (LIBs), sodium (SIBs), and potassium (KIBs)-ion batteries [15]. However, there are certain challenges in using such materials in actual applications, such as the complexity of obtaining higher power density and high efficiency while also achieving time, safety issues, and aging effects [16,17].

Supercapacitors (SCs) are often divided into three types based on their composition, structure, and operating principle: hybrid ion

* Corresponding authors at: Department of Materials and Optoelectronic Science, College of Semiconductor and Advanced Technology Research, Center of Crystal Research, National Sun Yat-Sen University, Kaohsiung 804, Taiwan.

E-mail addresses: mgamal.eldin12@aun.edu.eg (M.G. Mohamed), kuosw@faculty.nsysu.edu.tw (S.-W. Kuo).

<https://doi.org/10.1016/j.eurpolymj.2023.111980>

Received 19 January 2023; Received in revised form 26 February 2023; Accepted 5 March 2023

Available online 9 March 2023

0014-3057/© 2023 Elsevier Ltd. All rights reserved.

capacitors (HICs), electric double-layer capacitors (EDLCs), and asymmetric capacitors (ACs). Such capacitors provide certain advantages such as long-term performance at high current densities, that is, the number of repeated cycles for charging and discharging lasts for an infinite number of cycles [18–20], and high coulombic efficiency [21,22]. Such exceptional qualities make SCs excellent candidates for electrical energy storage devices [23–25]. Moreover, these devices have been designed specifically to store energy by creating an electrical double layer at the junction of a liquid electrolyte and solid porous electrode [26]. The majority of these SCs fall into one of two categories: non-faradaic processes (such as EDLCs), which rely on the accumulation of electrical charge at the electrode–electrolyte interface, and faradaic processes (such as pseudocapacitors) that occur at the substrate surface of heteroatom-doped carbon materials, conductive polymers, and metal oxide/hydroxide systems, which feature rapid redox reactions [27–29].

Conjugated microporous polymers (CMP), since their discovery by the Cooper group, are commonly known as promising materials among other organic polymers owing to their attractive properties such as microporous structure and extendable π -conjugation network in the skeleton structure, which are used for various kinds of applications, including the storage of gases, catalysis, energy, and metal ion sensing [30–40]. Earlier studies provided information that using these polymers has been effective for supercapacitors and has demonstrated outstanding electrochemical performance [17–19]. CMPs materials may be formed with various architectures and characteristics because of the extensive range of extensible construction blocks during reactions [41–45]. For instance, CMPs have been created via oxidative polymerization and traditional coupling techniques such as Suzuki–Miyaura, Sonogashira–Hagihara, and Yamamoto coupling [46–50]. On the other hand, organic and polymeric luminophores are intriguing materials used in a variety of applications, including plastic lasers, light-emitting diodes, fluorescent chemosensors, and fluorescent probes [51–57]. Moreover, scientists have created various luminescent materials to meet the requirements of fluorescent organic dyes, fluorescent proteins, and quantum dots. Additionally, numerous luminescent organic compounds with heterocyclic or benzene units exhibit a quenching effect upon the addition of various analytes via aggregation [55,56]. Most fluorescent polymeric materials use benzene or heterocyclic rings as their primary emissive components [55,56]. Considering that CMPs also have a highly fluorescent nature, they can be easily prepared and modified for suitable applications [56]. The construction of fluorescent POPs with high luminescence densities can be facilitated using large π -conjugated units and assembled π -conjugated systems as building blocks [56]. More importantly, with tunable emission properties and space to attach many fluorophore units, we substituted various functional units with porous structures. Herein, the efficient Suzuki coupling reaction has been used to prepare different conjugated microporous polymers (CMPs) [namely, Py-F, TPE-F, and TBN-CMPs] containing F, Py, TPE, and TBN, respectively. The molecular structure, morphology, porosity, and thermal stability of these materials were carefully investigated using FTIR, BET, TGA, SEM, TEM, and solid-state NMR measurements.

2. Experimental section

2.1. Materials

Dichloromethane (DCM), F-B(OH)₂, bromine solution (Br₂), pyrene (Py), potassium carbonate (K₂CO₃), 4-bromophenylboronic acid [BrBzB(OH)₂], and Pd(PPh₃)₄ were purchased from Sigma–Aldrich. Methanol (MeOH), iron chloride (III), and acetic acid (AcOH) were ordered from Acros. 1,3,6,8-Tetrabromopyrene (Py-Br₄), and tetraphenylethene (TPE) were produced using previously published methods [58–60]. PbNO₃, CuCl₂, ZnCl₂, HgCl₂, NiCl₂, COCl₂, FeCl₂, and MnCl₂ were purchased from Sigma–Aldrich.

2.2. Synthesis of 1,3,6,8-tetrakis(4-bromophenyl)pyrene (Py-Ph-Br₄)

To synthesize Py-Ph-Br₄, a combination of BrBzB(OH)₂ (3.6 g, 22 mmol), K₂CO₃ (4.26 g, 30.8 mmol), Py-Br₄ (2 g, 3.8 mmol), and Pd(PPh₃)₄ (0.80 g, 0.68 mmol) was taken under vacuum condition and was degassed subsequently. After adding 50 mL of 1,4-dioxane, the mixture was maintained at approximately 100 °C for 48 h. Finally, after 48 h, the residue was gently removed by filtering and washed with suitable solvents such as MeOH and H₂O. The obtained yellow product from the filtration was subsequently dried for a couple of days at 80 °C to obtain a fine yellow powder [Scheme S1], and its chemical structure was confirmed using FTIR (KBr, cm⁻¹): 3027, 1597, 676. ¹H NMR (Fig. S1): 8.25–7.42 (aromatic protons). HR-FD-MS: *m/z*: 822.90 (Fig. S2). Py-Ph-Br₄ had T_{d10} = 281 °C and char yield = 48 wt% (by TGA analysis, Fig. S3).

2.3. Synthesis of Tetrakis(4-bromophenyl)ethylene (TPE-Br₄)

DCM (150 mL), TPE (4.0 g, 12.04 mmol), and acetic acid (50 mL) were directly added to the round-bottom flask and covered with aluminum foil to change the mixture to 0 °C using a salt-ice-water solution. Next, Br₂ (4.0 g, 50 mmol) was added to the reaction solution under constant stirring, and the solution was stirred overnight. To obtain the crude product, the solution was washed with sodium thiosulfate, extracted using DCM, and dried with MgSO₄. The formed precipitate was recrystallized twice with ethanol and air-dried to provide TPE-Br₄ as a white solid [Scheme S2]. At last, TPE-Br₄ was confirmed using FTIR (KBr, cm⁻¹): 3051, 1572. ¹H NMR (500 MHz, CDCl₃, Fig. S4): 7.27 (8H), 6.86 (8H). ¹³C NMR (125 MHz, CDCl₃, Fig. S5): 142.30–121.80. T_{d10} = 354 °C and char yield = 0.7 wt% (by TGA analysis, Fig. S6).

2.4. Synthesis of 2,7,10,15-Tetrabromotetrazabenzonaphthalene (TBN-Br₄)

TPE-Br₄ (1.0 g, 1.54 mmol) was subsequently mixed in dry DCM (40 mL) under the presence of a nitrogen atmosphere. Following that, a septum was used to add solutions of FeCl₃ (4.54 g, 27.2 mmol) in dry nitromethane (10 mL) to the reaction mixture. The materials were warmed at reflux for approximately 4 h before being cooled to room temperature. The reaction was stopped by adding 50 mL of methanol. The chemical components were then extracted with CHCl₃, washed with a diluted NaHCO₃ solution, and evaporated until dryness to obtain TBN-Br₄ as a yellow solid (0.71 g, 76%, Scheme S3); FTIR (KBr, cm⁻¹, Fig. S7): 3078 (aromatic C–H), 1594 (C=C), 591. ¹H NMR (500 MHz, CDCl₃, Fig. S8): 7.77 (s, 4H), 8.42 (s, 4H), 8.73 (s, 4H). ¹³C NMR (500 MHz, CDCl₃, Fig. S9): 135.70, 132.40, 127.80, 119.20, 103.50, 101.60. T_{d10} = 431 °C and char yield = 46 wt% (by TGA analysis, Fig. S10).

2.5. Synthesis of Py-F CMP

In 150 mL of a two-necked flask, F-B(OH)₂ (212 mg, 0.36 mmol), Pd (20.8 mg, 0.018 mmol), Py-Ph-Br₄ (150 mg, 0.18 mmol), and K₂CO₃ (194 mg, 1.4 mmol) were added to DMF (15 mL)/H₂O (5 mL) to the reaction mixture. Then, the reaction solution was refluxed at 90 °C for 72 h under N₂. The precipitate material would be thoroughly filtered and washed with THF and acetone. Finally, the deep dark green solid was dried at 100 °C (0.24 g, 66%).

2.6. Synthesis of TPE-F CMP

The synthesis of TPE-F CMP was carried out using the same procedures used for the preparation of Py-F CMP; TPE-Br₄ (150 mg, 0.23 mmol), F-B(OH)₂ (270 mg, 0.46 mmol), K₂CO₃ (254 mg, 1.84 mmol), and Pd (26 mg, 0.023 mmol) to afford a light-green solid (0.29 g, 70%).

2.7. Synthesis of TBN-F CMP

The synthesis of TBN-F CMP was carried out using the same procedures used for the preparation of Py-F CMP; TBN-Br₄ (100 mg, 0.16 mmol), F-B(OH)₂ (188 mg, 0.32 mmol), K₂CO₃ (177 mg, 1.28 mmol), and Pd (18 mg, 0.016 mmol) to give a light-green solid (0.21 g, 72%).

2.8. Sensing of Pb²⁺ ions

To investigate the sensing analytes, initially, the known amount of Py-F CMP (1 mg/mL) was taken and partially suspended in ultra-pure DI water via ultrasonication method for 30 mins. Finally, the partially dispersed clear Py-F CMP were collected separately in a different centrifuge tube. Then the known volume of the above solution [300 μL] was taken, and the different concentrations of Pb²⁺ (200 μL; 0.10–500 μM) were included alongside followed by observing the mixture at the ambient condition with shaking under vortex. After 5–10 mins, the resultant final mixed solution was taken in the quartz cuvette (1 mL volume), and their PL emission curve was recorded by fixing the excitation wavelength at 360 nm.

2.9. Interference assay for Pb⁺ ion

To know the effect of Pb²⁺ sensing with Py-F CMP, the same procedure mentioned above for Py-F CMP was executed. But substituting various other metal ions such as Fe²⁺, Zn²⁺, Co²⁺, Mn²⁺, Cr³⁺, Cu²⁺, Hg⁺, and Ni²⁺ [500 μM] in the place of Pb²⁺. The interference assay of the other two probes such as TPE-F CMP and TBN-F CMP has also evolved simultaneously accordingly to the protocol applied for Py-F CMP.

3. Results and discussion

3.1. Synthesis and characterization of Py-F CMP, TPE-F CMP, and TBN-F CMP

The target Py-F, TPE-F, and TBN-F CMPs was constructed and prepared by using the Suzuki coupling reaction, and the synthetic route of F-based CMPs is shown in Fig. 1. The Py-Ph-Br₄ monomer was prepared through the reaction of Py-Br₄ with BrBzB(OH)₂ in the presence of 1,4-dioxane and Pd as the catalyst [Scheme S1]. The TPE molecule was

brominated with neat Br₂ in the mixture of DCM and AcOH to access TPE-Br₄ as a white powder [Scheme S2]. Finally, TPE-Br₄ has converted to TBN-Br₄ [Scheme S3] in the presence of DCM/CH₃NO₂/catalytic amount of anhydrous FeCl₃. The chemical structure of the synthesized Py-Ph-Br₄, TPE-Br₄, and TBN-Br₄ monomers were proven by using FTIR and NMR spectroscopy [as shown in the experimental part]. The absorption peaks at 3080, 3060, and 3078 cm⁻¹ in the FTIR spectra of all synthesized monomers are attributed to the aromatic CH stretching [Figs. S11–S13]. The peaks were centered at 1589, 1573, and 1620 cm⁻¹ corresponding to the C=C group in the Py-Ph-Br₄, TPE-Br₄, and TBN-Br₄ structures. The FTIR spectrum of the F-B(OH)₂ [Fig. S11] featured the absorption bands at 3348, 2920, and 1598 cm⁻¹ for the hydroxyl group (OH), aromatic CH stretching, and C=C groups, respectively. The synthetic route of the F-based CMPs is shown in Fig. 1. The reaction of F-B(OH)₂ with Py-Ph-Br₄, TPE-Br₄, and TBN-Br₄ in the presence of K₂CO₃ and Pd in a mixture of DMF/H₂O to access Py-F CMP, TPE-F CMP and TBN-F CMP, respectively, as a green powder with a moderate yield up to 70%.

The presence of functional groups in the obtained F-based CMPs was determined using FTIR analyses, as presented in Fig. 2(a) and Figs. S11–S13. As shown in Fig. 2(a), the absorption peaks of Py-F CMP appear at 1608 and 2920 cm⁻¹ represent the involvement of C=C and aliphatic C–H group, respectively. The FTIR profile of TPE-F CMP shows a similar type of absorption peak that emerged at 2924, 1467, and 1605 cm⁻¹ indicating the involvement of the aliphatic C–H stretching, C=C along with the aromatic ring. For the TBN-F CMP sample, the major functional groups located at 1466, 1607, and 2921 cm⁻¹ are due to the existence of aromatic and aliphatic CH units in the F moiety. In addition, the absorption peaks of the C–Br and B–O groups were completely disappeared in all FTIR profiles of F-CMPs materials [Fig. 2(a) and Figs. S11–S13]. All these absorption bands in their FTIR spectra confirm the successful synthesis of these F-based CMPs. ¹³C solid-state NMR spectra of F-based CMPs are shown in Fig. 2(b). The peaks located in the range 44–72 ppm and 96–164 ppm for Py-F CMP, TPE-F CMP, and TBN-F CMP correspond to their hexyl carbons in the F unit and aromatic ring carbons in their framework, respectively. The above FTIR and NMR analyses confirmed the successful synthesis of F-based CMPs [Fig. 1]. Fig. 2(c) displays the thermal stability of Py-F CMP, TPE-F CMP, and TBN-F CMP. The TGA analyses of three new F-based CMPs were tested under N₂ and indicated 10% weight losses of Py-F CMP, TPE-F CMP, and TBN-F CMP were 410, 409, and 418 °C, respectively. Furthermore, the

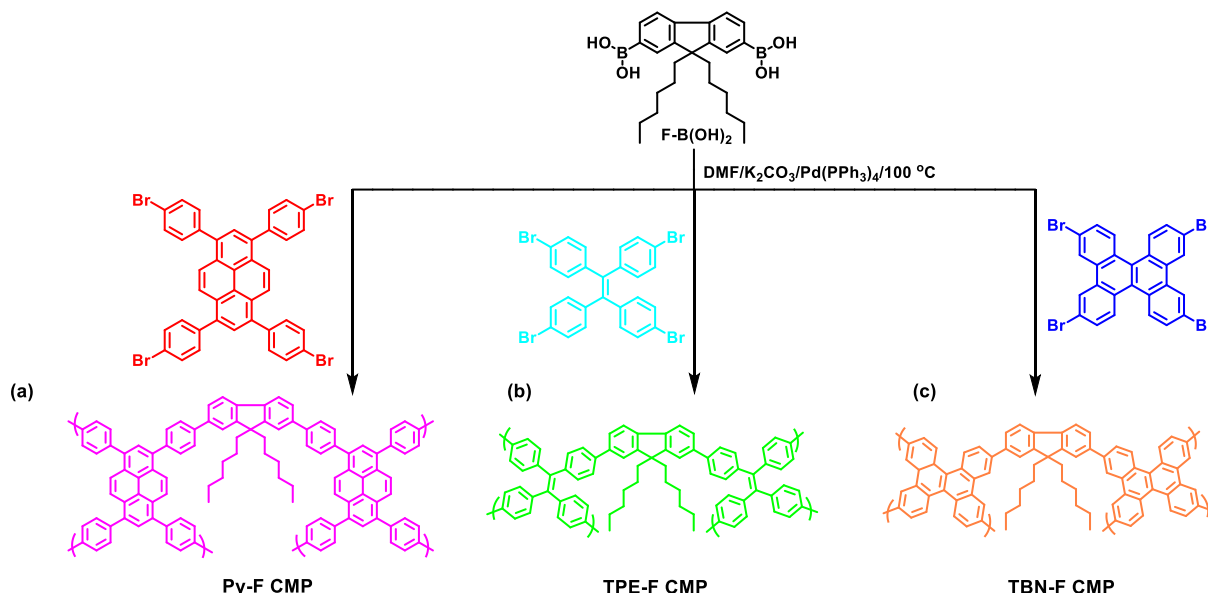


Fig. 1. Synthesis of the (a) Py-F, (b) TPE-F, and (c) TBN-F CMPs.

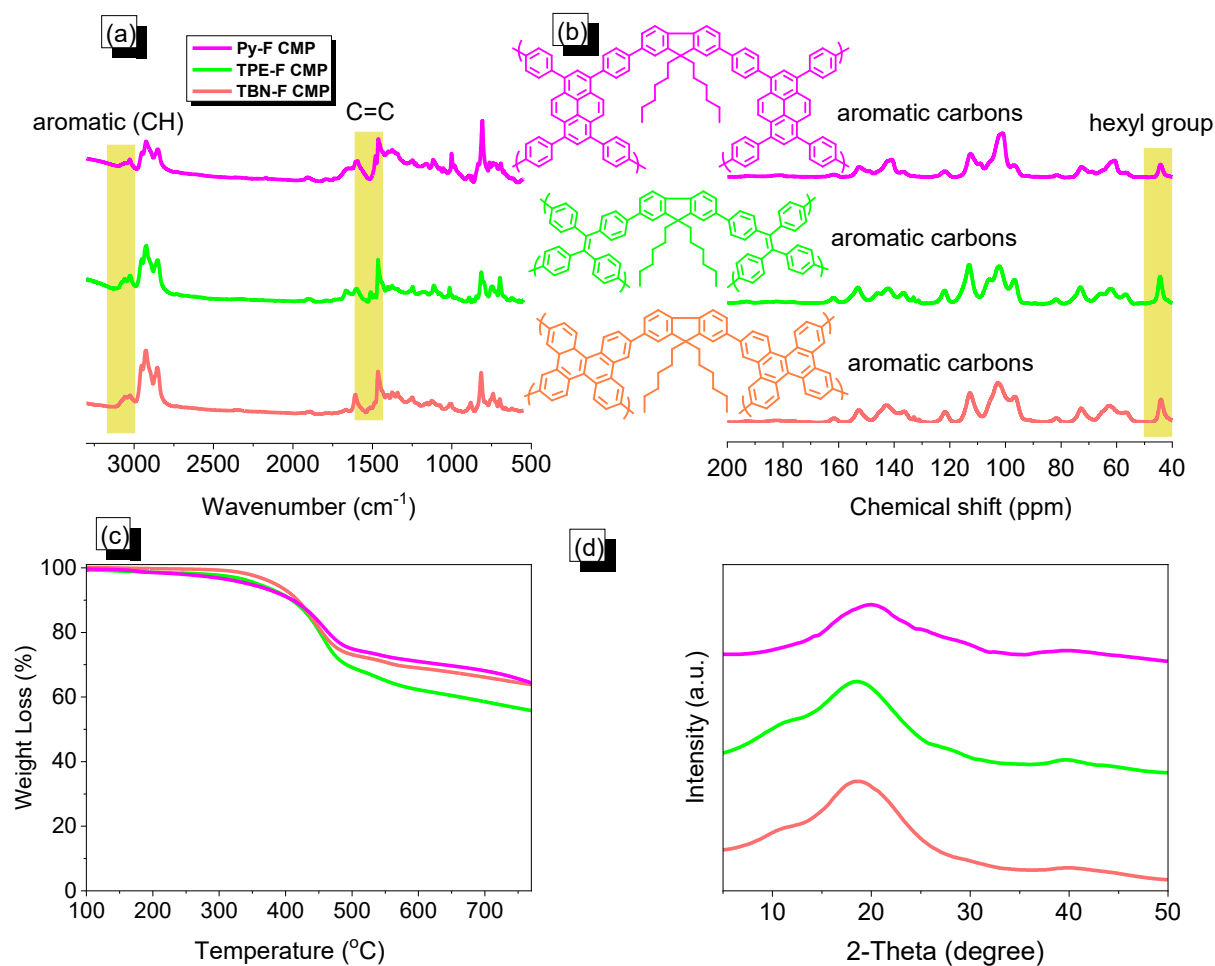


Fig. 2. (a) FTIR, (b) solid-state ¹³C NMR, (c) TGA traces, and (d) XRD patterns of the Py-F, TPE-F, and TBN-F CMPs.

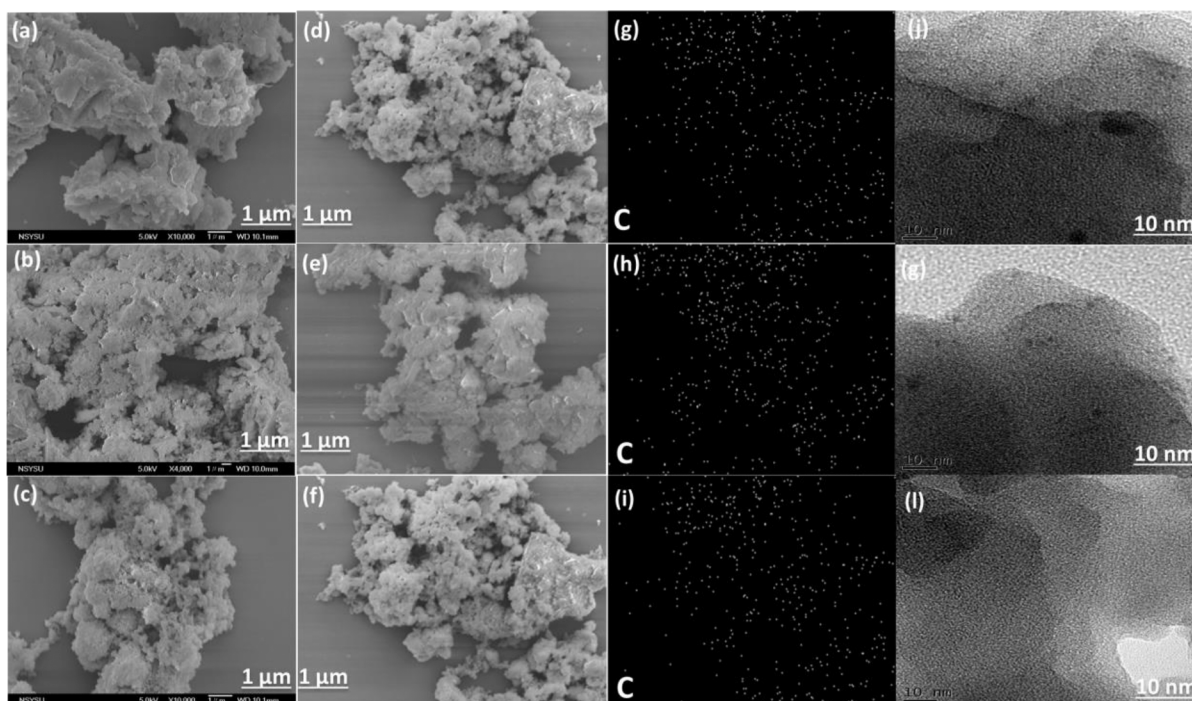


Fig. 3. (a-c) SEM images, EDS mapping (d-i) and (j-l) TEM images of Py-F (a, d, g, j), TPE-F (b, e, h, g) and TBN-F CMPs (c, f, i, l).

char yields at 800 °C for Py-F, TPE-F, and TBN-F CMPs were found to be 62.8, 55.0, and 63.3 wt%, respectively. Based on TGA measurements, our obtained F-based CMPs possessed good thermal stability due to their high crosslinking density. The amorphous character of the F-based CMPs materials was investigated by powder X-ray diffraction (PXRD) [Fig. 2 (d)].

The morphologies of the porous Py-F CMP, TPE-F CMP, and TBN-F CMP were further examined using field emission scanning electron microscopy (FE-SEM) and high-resolution transmission electron microscopy (HR-TEM) [Fig. 3]. FE-SEM imaging revealed that all three F-CMPs included tiny aggregated spherical particles [Fig. 3(a)–(c)]. The abundance of bright and alternating dark patches on the HR-TEM images [Fig. 3(d)–(f)] suggested that all of the F-CMPs had porous networks. The EDS analysis of the F-based CMPs [Fig. 3] verified the presence of carbon atoms and their uniform distribution across the framework of the F-CMPs.

The pore size, total pore volume, and surface area of the as-synthesized F-based CMP materials were measured using nitrogen adsorption–desorption analyses. The nitrogen adsorption–desorption isotherms of the F-based CMP materials are shown in Fig. 4, where the isotherms were characterized as type I with minor hysteresis loops for Py-F and TPE-F CMPs [Fig. 4(a) and (b)] and as type IV isotherms with large hysteresis loops for TBN-F CMP framework [Fig. 4(c)]. The rapid quantity of N₂ absorption in the low and high-pressure zone indicates the existence of microporosity and interparticle porosity in the as-synthesized TBN-F CMP framework. The surface areas of the Py-F,

TPE-F, and TBN-F CMPs materials are calculated to be 40, 55, and 200 m² g⁻¹, respectively, using Brunauer Emmett Teller (BET) method. The comparable pore volumes of Py-F, TPE-F, and TBN-F CMPs frameworks determined repeatedly are 0.15, 0.18, and 0.68 cm³ g⁻¹. Using NLDFT (nonlocal density functional theory) approach, the corresponding average pore sizes of Py-F, TPE-F, and TBN-F CMPs were found to be ca. 2.7, 2.4 and 1.8 nm, respectively, as indicated in Fig. 4(d)–(f).

3.2. Fluorescence properties and metal sensing of Py-F CMP, TPE-F CMP, and TBN-F CMP

To understand their fluorescence properties in their highly concentrated powdered CMP with Py-F, TBN-F, and TPE-F were taken in a centrifuge tube and suspended in ultrapure DI water under sonication treatment. Then, after 5–10 mins, the dispersed sample solution was changed in another centrifuge tube for other experimental analysis. To characterize the optical properties of those CMP 0.5 mL of each solution were used, and their emission curve was checked using a fluorescence spectrophotometer (HITACHI F7000). As per Fig. 5(a–c), all three kinds of CMP show strong fluorescence intensity individually at around 486, 488, and 526 nm for Py-F CMP, TBN-F CMP, and TPE-F CMP, respectively. In addition, the obtained emission wavelength shows similar properties like of earlier reported materials [61–64]. In addition, the obtained emission wavelength was independent of their corresponding excitation wavelength (from 300 to 480 nm), which was opposite to that of other reported probes that take them to other exciting applications.

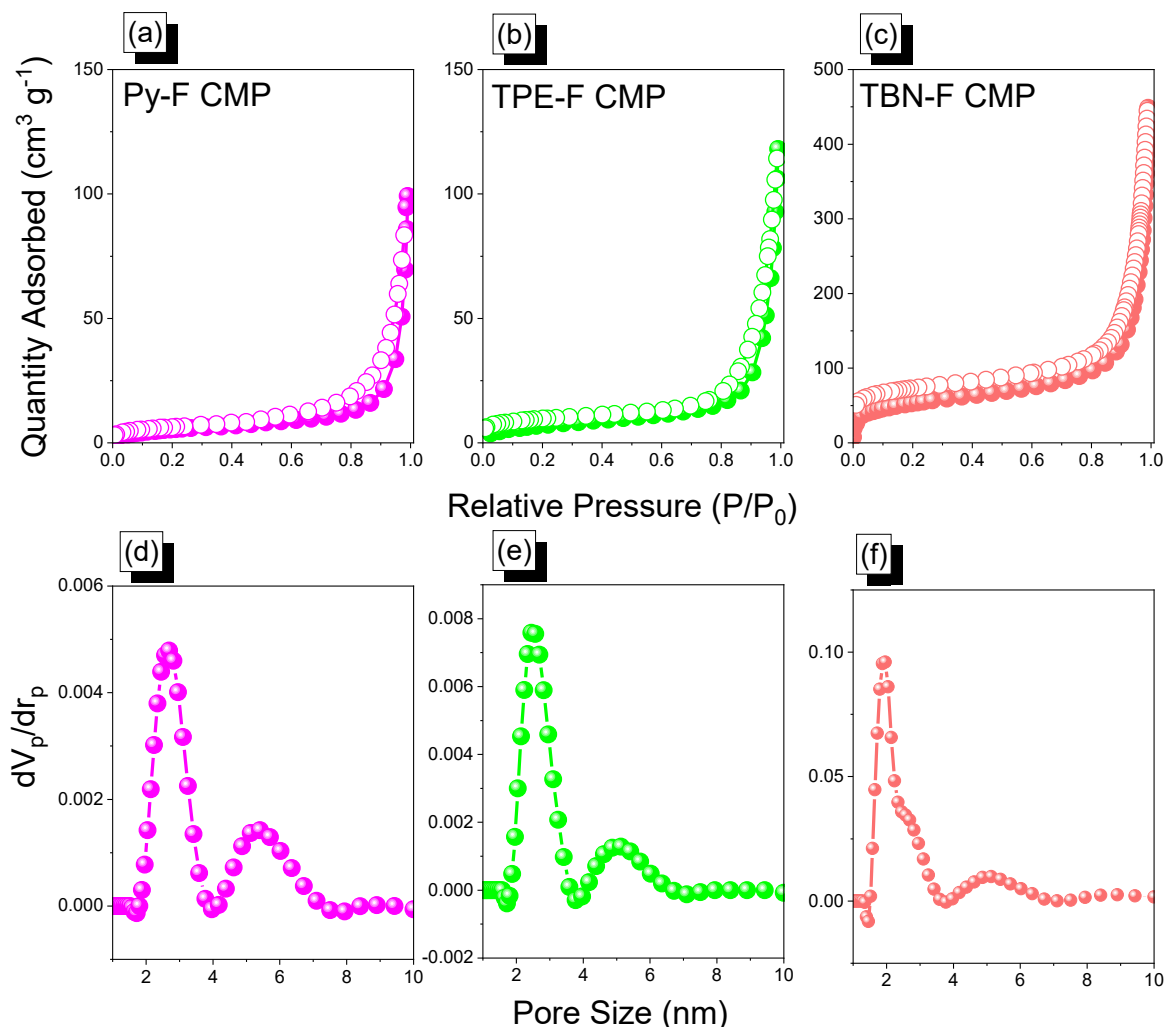


Fig. 4. N₂ sorption isotherms, and pore size curves profiles of the Py-F (a, d), TPE-F (b, e), and TBN-F CMPs (c, f).

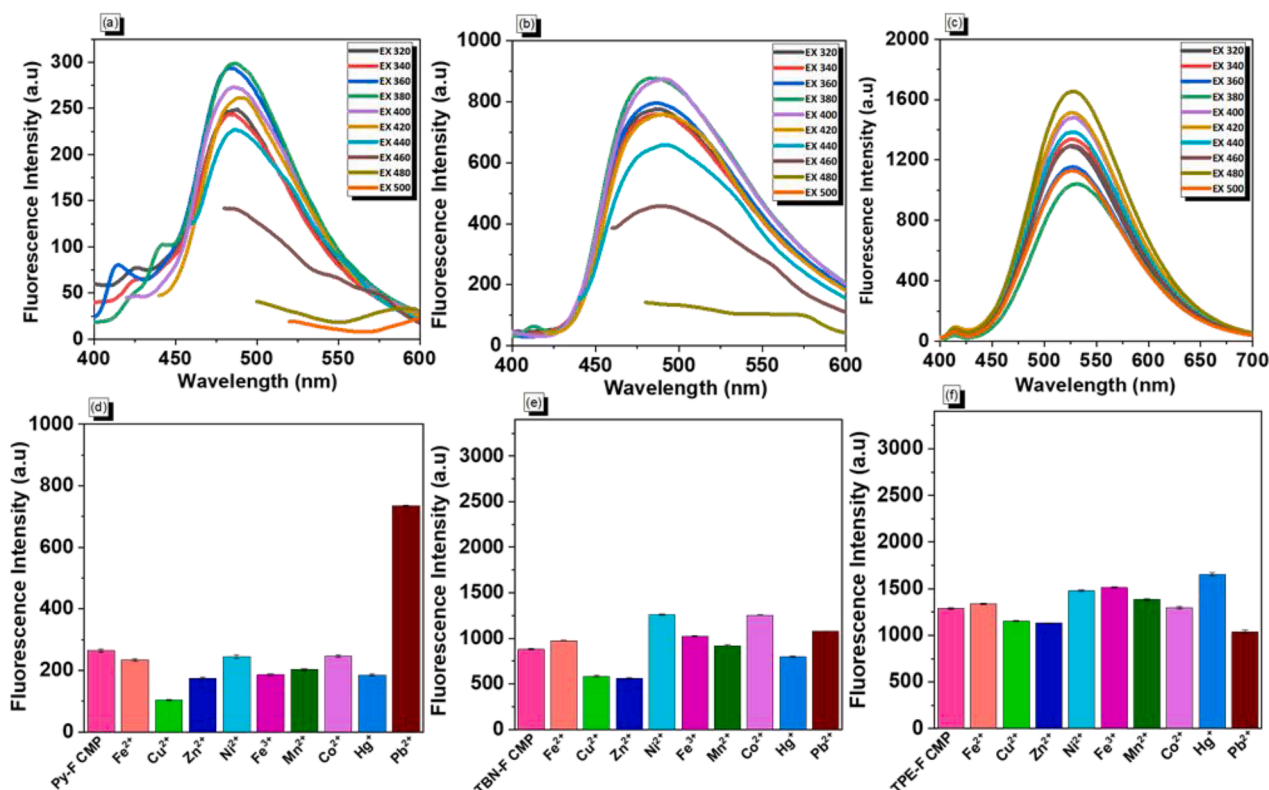


Fig. 5. (a-c) optical characterization: Excitation independent fluorescence spectrum (a) Py-F, (b) TBN-F, and (c) TPE-F CMPs. (d-f) Selectivity studies of the proposed probe towards Pb^{2+} of (d) Py-F, (e) TBN-F, and (f) TPE-F CMPs.

Based on the absolute calculation methods the QY % (measured with Edinburgh FS5 spectrofluorometer, UK) for the synthesized CMPs are known to be 1.2, 2.1 and 1.7% for Py-F CMP, TPE-F CMP, and TBN-F CMP, respectively. Next, the above-mentioned F-CMPs were evidenced separately from different kinds of metal ions like Fe^{2+} , Zn^{2+} , Co^{2+} , Mn^{2+} , Fe^{3+} , Cu^{2+} , Hg^{2+} , and Ni^{2+} , and the results in more fluorescence fluctuating were observed for TPE-F CMP and TBN-F CMP than that of Py-F-CMP [Fig. 5(d-f)]. At last, solid evidence was obtained and conclusions were brought to focus only on Py-F-based CMP and to analyze the selective metal ions like Pb^{2+} .

Therefore, considering the high selectivity of the Py-F CMP toward Pb^{2+} we next determined the various concentrations of Pb^{2+} , as per Fig. 6(a) at elevated concentration [0.1–500 μM], the Pb^{2+} continuously enhances their emission intensity that was recorded at 488 nm. Plotting the fluorescence intensity value with the multiple concentrations of Pb^{2+} gave linear calibration curves (Fig. S14). It should be noted that the stern Volmer fitting plot (Fig. 6(b)) indicates that the sensing was linearly fitted at the range of 0.1–2.0 μM range. The correlation coefficients (R^2) for this range were 0.9752 for determining Pb^{2+} . The detection limit (LOD) of Pb^{2+} was calculated using the Eq. (1) given below.

$$LOD = 3 \times \sigma / K \quad (1)$$

Here, σ indicates the standard deviation of blank measurements five times. K represents the slope of the emission curve for excitation at 360 nm versus the concentration of Pb^{2+} ion, and the detection limit of the Py-F CMP was estimated to be 0.01 μM [Table S1].

3.3. Electrochemical analysis of F-Based CMPs materials [Py-F, TPE-F, and TBN-F CMPs]

We conducted galvanostatic charge/discharge (GCD) experiments and cyclic voltammetry (CV) testing on our as-prepared F-based CMPs to assess their electrochemical performance. Between -1.0 and 0.0 V, we investigated the CV curves of the Py-F, TPE-F, and TBN-F CMPs,

respectively [Fig. 7(a-c)]. Every F-based CMP displayed almost rectangle CV patterns with little humps at lower potentials, which supported EDLC behavior [65–68]. In addition, the current densities increased without affecting the shapes when the scan rate was increased from 5 to 200 $mV s^{-1}$. Furthermore, all of the CMPs having F moieties showed enhanced rate capabilities, reliabilities, and kinetic profiles since the current densities increased when the scan rate was increased from 5 to 200 $mV s^{-1}$ without affecting the shapes of the CV profiles. Most of the variation in electrochemical properties between the materials can be attributed to the porous structure and the availability of micro- and mesoporosity, which all guaranteed great access of the electrolyte to the electrode surface, resulting in rapid mass transport, and improved electrochemical performance [65–68]. The porous design of our F-based CMPs framework provides diffusing channels and more efficient electrolyte ion transport, improving the electrochemical efficiency [65]. Moreover, we evaluated the GCD performance of the Py-F, TPE-F, and TBN-F CMPs with current densities ranging from 0.5 to 20 $A g^{-1}$. The nearly triangular GCD profiles of all the CMPs, displayed a little twist along the discharge curve, indicating the combined effects of EDLC and pseudo-capacitance behavior [Fig. 7(d-f)].

Based on the GCD profiles, the specific capacitances of each F-based CMP were estimated [Fig. 8(a)]. The specific capacitance values for Py-F CMP were respectively 133.35, 43.08, 20.82, 14.46, 9.60, 7.63, 6.30, 5.55, and 5.2 $F g^{-1}$, for TPE-F CMP, they were 100.75, 39.9, 17.56, 12.81, 9.05, 7.42, 6.10, 5.07, and 4.52 $F g^{-1}$, whereas, for TBN-F CMP, they were 194.15, 56.2, 25, 18.51, 13.85, 11.69, 10.0, 8.55, and 8.05 $F g^{-1}$, at current densities of 0.5, 1, 2, 3, 5, 7, 10, 15, and 20 $A g^{-1}$, respectively. As a whole, TBN-F CMP outperformed all other samples regarding rate capability. This behavior may be attributed to the TBN-F CMP's porous structure, which is mesoporous in nature as illustrated in Fig. 4(f), which enables electrolyte ions to permeate into the inner active sites at greater current densities, improving rate performance. Similarly, we studied the cycling stability profiles of all F-based CMPs materials using GCD evaluation at a current density of 10 $A g^{-1}$ for 2000 cycles to

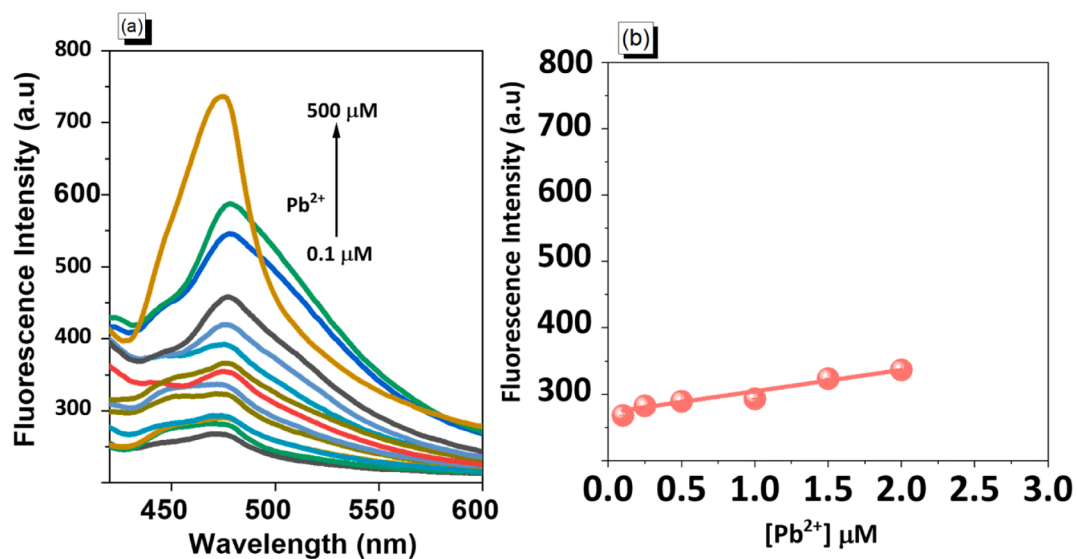


Fig. 6. Sensing of Py-F CMP toward Pb^{2+} : (a) Quantification of Pb^{2+} ion with different concentrations [0.1 μM –200 μM] and (b) the Stern Volmer plot in the concentration range from 0.1–2.0 μM .

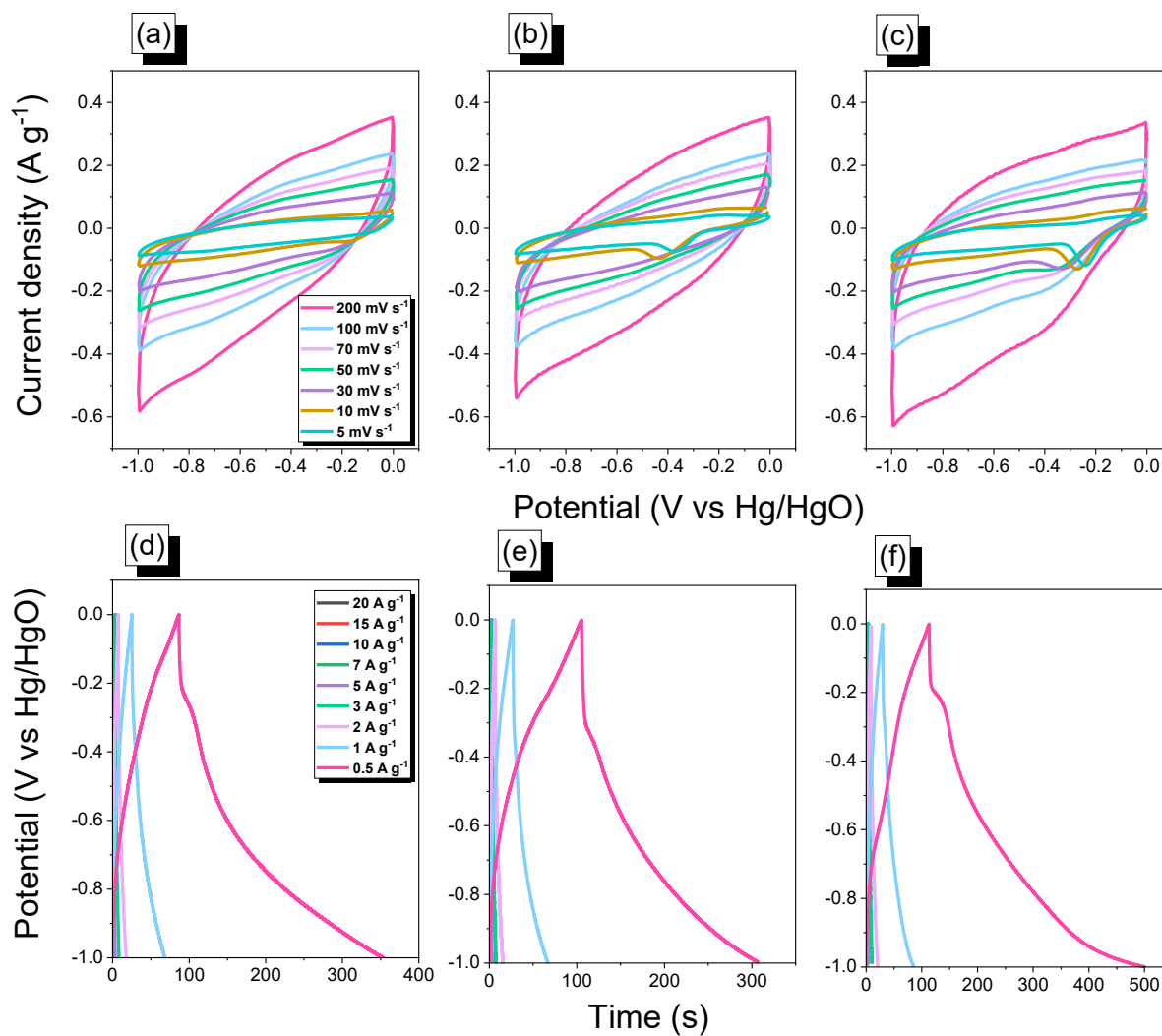


Fig. 7. (a-c) Cyclic voltammetry curves and (d-f) galvanostatic charge–discharge curves of Py-F (a, d), TPE-F (b, e), and TBN-F CMPs (c, f).

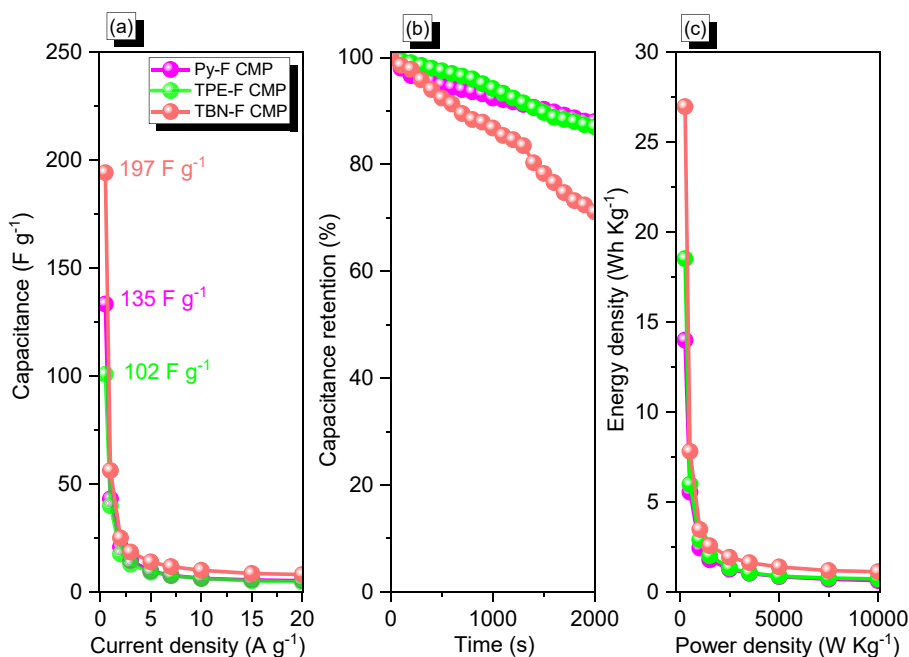


Fig. 8. (a) Specific capacitance, (b) long cycling stability, and (c) Ragone profiles of Py-F, TPE-F, and TBN-F CMPs.

assess the stability of these electrode materials during extensive cycling testing [Fig. 8(b)]. Py-F, and TPE-F, TBN-F CMPs have managed to retain 87.0, 71.1, and 9 % of their initial capacity, demonstrating their exceptional stability in aqueous 1 M KOH electrolyte as electrode material for energy storage devices. Finally, the energy density of the Py-F CMP, TPE-F CMP, and TBN-F CMP was calculated to be 14, 19, and 27 Wh kg⁻¹, respectively [Fig. 8(c)].

4. Conclusion

To conclude, the design and construction of fluorescent three novel 2D F-based CMPs containing fluorene moieties were carried out through Suzuki coupling. The Py-F and TBN-F CMPs both showed high values of T_{d10} (410 and 418 °C, respectively), with char yields of up to 62 wt%, according to TGA. Among all synthesized F-CMPs, the TBN-F CMP had a high surface area of 200 m² g⁻¹ and a pore volume of 0.68 cm³ g⁻¹. In addition, the Py-F CMP with their excellent optical behavior was specifically and selectively used to detect Pb²⁺ ion. On the basis of these three F-CMPs, we then assessed the electrochemical performance of the three-electrode system. Compared to other porous polymers utilized as electrodes, the Py-F CMP and TBN-F CMP in the three-electrode findings produced specific capacities of 135 and 197 F g⁻¹, respectively, at a 0.5 A g⁻¹ and higher cycle stability up to 90% [Table S2]. Because of their acceptable porosity characteristics, outstanding capacitances, straightforward manufacture, and diverse morphologies, our F-linked CMPs appear to be viable candidate materials for use in metal ion sensing and energy storage.

CRedit authorship contribution statement

Mohamed Gamal Mohamed: Conceptualization, Methodology, Data curation, Writing – original draft, Supervision. **Huan-Yu Hu:** Formal analysis, Data curation. **Manivannan Madhu:** Data curation, Writing – original draft. **Maha Mohamed Samy:** Conceptualization. **Islam M.A. Mekhemer:** Conceptualization. **Wei-Lung Tseng:** Conceptualization. **Ho-Hsiu Chou:** Data curation. **Shiao-Wei Kuo:** Funding acquisition, Project administration, Supervision.

Declaration of Competing Interest

The authors declare that they have no known competing financial interests or personal relationships that could have appeared to influence the work reported in this paper.

Data availability

The data that has been used is confidential.

Acknowledgments

This study was supported financially by the Ministry of Science and Technology, Taiwan, under contracts NSTC 110-2124-M-002-013 and 111-2223-E-110-004. The authors thank the staff at National Sun Yat-sen University for their assistance with the TEM (ID: EM022600) experiments.

Appendix A. Supplementary material

Supplementary data to this article can be found online at <https://doi.org/10.1016/j.eurpolymj.2023.111980>.

References

- [1] M.M. Samy, M.G. Mohamed, S.U. Sharma, S.V. Chaganti, J.T. Lee, S.W. Kuo, An Ultrastable Tetrabenzonaphthalene-Linked conjugated microporous polymer functioning as a high-performance electrode for supercapacitors, *J. Taiwan Inst. Chem. Eng.* (2023), 104750, <https://doi.org/10.1016/j.jtice.2023.104750>.
- [2] M. Gao, M.J. Zheng, A.F.M. EL-Mahdy, C.W. Chang, Y.C. Su, W.H. Hung, S.W. Kuo, L.H. Yeh, A Bioinspired ionic diode membrane based on Sub-2 nm covalent organic framework channels for ultrahigh osmotic energy generation, *Nano Energy* 105 (2023), <https://doi.org/10.1016/j.nanoen.2022.108007>.
- [3] M.M. Samy, M.G. Mohamed, S.W. Kuo, Pyrene-functionalized tetraphenylethylene polybenzoxazine for dispersing single-walled carbon nanotubes and energy storage, *Compos. Sci. Technol.* 199 (2020), 108360, <https://doi.org/10.1016/j.compscitech.2020.108360>.
- [4] S. Liu, L. Kang, J. Henzie, J. Zhang, J. Ha, M.A. Amin, M.S.A. Hossain, S.C. Jun, Y. Yamauchi, Recent advances and perspectives of battery-type anode materials for potassium ion storage, *ACS Nano* 15 (2021) 18931–18973, <https://doi.org/10.1021/acsnano.1c08428>.
- [5] Q. Wang, M. Zhu, G. Chen, N. Dudko, Y. Li, H. Liu, L. Shi, G. Wu, D. Zhang, High-performance micro-sized Si anodes for lithium-ion batteries: insights into the

- polymer configuration conversion mechanism, *Adv. Mater.* 34 (2022) 2109658, <https://doi.org/10.1002/adma.202109658>.
- [6] D. Chen, K. Jiang, T. Huang, G. Shen, Recent advances in fiber supercapacitors: materials, device configurations, and applications, *Adv. Mater.* 32 (2020) 1901806, <https://doi.org/10.1002/adma.201901806>.
- [7] F. Raffik, H. Gualous, R. Gallay, A. Crausaz, A. Berthon, Frequency, thermal and voltage supercapacitor characterization and modeling, *J. Power Sources* 165 (2007) 928–934, <https://doi.org/10.1016/j.jpowsour.2006.12.021>.
- [8] W. Lyu, C. Yan, Z. Chen, J. Chen, H. Zuo, L. Teng, H. Liu, L. Wang, Y. Liao, Spirobifluorene-based conjugated microporous polymer-grafted carbon nanotubes for efficient supercapacitive energy storage, *ACS Appl. Energy Mater.* 5 (2022) 3706–3714, <https://doi.org/10.1021/acsaeam.2c00151>.
- [9] M.G. Mohamed, T.H. Mansoure, Y. Takashi, M.M. Samy, T. Chen, S.W. Kuo, Ultrastable porous organic/inorganic polymers based on polyhedral oligomeric silsesquioxane (POSS) hybrids exhibiting high performance for thermal property and energy storage, *Microporous Mesoporous Mater.* 328 (2021), 111505, <https://doi.org/10.1016/j.micromeso.2021.111505>.
- [10] X.C. Li, Y. Zhang, C.Y. Wang, Y. Wan, W.Y. Lai, H. Pang, W. Huang, Redox-active triazatruxene-based conjugated microporous polymers for high-performance supercapacitors, *Chem. Sci.* 8 (2017) 959–2965, <https://doi.org/10.1039/C6SC05532J>.
- [11] W. Septiani, Y.V. Kaneti, K.B. Fathoni, J. Wang, Y. Ide, B. Yulianto, B. Nugraha, H. K. Dipojono, A.K. Nanjundan, D. Golberg, Y. Bando, Y. Yamauchi, Self-assembly of nickel phosphate-based nanotubes into two-dimensional crumpled sheet-like architectures for high-performance asymmetric supercapacitors, *Nano Energy* 67 (2020), 104270, <https://doi.org/10.1016/j.nanoen.2019.104270>.
- [12] L. Li, F. Lu, R. Xue, B.L. Ma, Q. Li, N. Wu, H. Liu, W.Q. Yao, H. Guo, W. Yang, Ultrastable triazine-based covalent organic framework with an interlayer hydrogen bonding for supercapacitor applications, *ACS Appl. Mater. Inter.* 11 (2019) 26355–26363, <https://doi.org/10.1021/acsami.9b06867>.
- [13] M.M. Samy, M.G. Mohamed, A.F.M. El-Mahdy, T.H. Mansoure, K.C.W. Wu, S. W. Kuo, High-performance supercapacitor electrodes prepared from dispersions of tetrabenzonaphthalene-based conjugated microporous polymers and carbon nanotubes, *ACS Appl. Mater. Inter.* 13 (2021) 51906–51916, <https://doi.org/10.1021/acsami.1c05720>.
- [14] N.N. Loganathan, V. Perumal, B.R. Pandian, R. Atchudan, T.N.J.I. Edison, M. Ovinis, Recent studies on polymeric materials for supercapacitor development, *J. Storage Mater.* 49 (2022), 104149, <https://doi.org/10.1016/j.est.2022.104149>.
- [15] F. Wu, J. Gao, X. Zhai, M. Xie, Y. Sun, H. Kang, Q. Tian, H. Qiu, Hierarchical porous carbon microrods derived from albizia flowers for high performance supercapacitors, *Carbon* 147 (2019) 242–251, <https://doi.org/10.1016/j.carbon.2019.02.072>.
- [16] Z. Xu, S. Sun, Y. Han, Z. Wei, Y. Cheng, S. Yin, W. Cui, High-energy-density asymmetric supercapacitor based on a durable and stable manganese molybdate nanostructure electrode for energy storage systems, *Appl. Energy Mater.* 3 (2020) 5393–5404, <https://doi.org/10.1021/acsaeam.0c00393>.
- [17] L. Mei, J.C. Wei, Q. Duan, Construction of copper porphyrinlinked conjugated microporous polymer/carbon nanotube composite as flexible electrodes for supercapacitors, *J. Mater. Sci. Mater. Electron* 32 (2021) 24953–24963, <https://doi.org/10.1007/s10854-021-06952-w>.
- [18] K. Amin, N. Ashraf, L. Mao, C.F.J. Faul, Z. Wei, Conjugated microporous polymers for energy storage: Recent progress and challenges, *Nano Energy* 85 (2021), 105958, <https://doi.org/10.1016/j.nanoen.2021.105958>.
- [19] M.G. Mohamed, S.V. Chaganti, S.U. Sharma, M.M. Samy, M. Ejaz, J.T. Lee, K. Zhang, S.W. Kuo, Constructing conjugated microporous polymers containing the pyrene-4,5,9,10-tetraone unit for energy storage, *ACS Appl. Energy Mater.* 5 (2022) 10130–10140, <https://doi.org/10.1021/acsaeam.2c01842>.
- [20] M.M. Samy, M.G. Mohamed, S.W. Kuo, Conjugated microporous polymers based on ferrocene units as highly efficient electrodes for energy storage, *Polymers* 15 (2023) 1095, <https://doi.org/10.3390/polym15051095>.
- [21] S. Liu, L. Kang, J. Zhang, E. Jung, S. Lee, S.C. Jun, Structural engineering and surface modification of MOF-derived cobalt-based hybrid nanosheets for flexible solid-state supercapacitors, *Energy Storage Mater.* 32 (2020) 167–177, <https://doi.org/10.1016/j.ensm.2020.07.017>.
- [22] M.G. Mohamed, S.V. Chaganti, M.S. Li, M.M. Samy, S.U. Sharma, J.T. Lee, M. H. Elsayed, H.H. Chou, S.W. Kuo, Ultrastable porous organic polymers containing thianthrene and pyrene units as organic electrode materials for supercapacitors, *ACS Appl. Energy Mater.* 5 (2022) 6442–6452, <https://doi.org/10.1021/acsaeam.2c00942>.
- [23] M.G. Mohamed, S.U. Sharma, C.H. Yang, M.M. Samy, A.A.K. Mohammed, S. V. Chaganti, J.T. Lee, S.W. Kuo, Anthraquinone-enriched conjugated microporous polymers as organic cathode materials for high-performance lithium-ion batteries, *ACS Appl. Energy Mater.* 4 (2021) 14628–14639, <https://doi.org/10.1021/acsaeam.1c03270>.
- [24] C. Young, T. Park, J.W. Yi, J. Kim, M.S.A. Hossain, Y.V. Kaneti, Y. Yamauchi, Advanced functional carbons and their hybrid nanoarchitectures towards supercapacitor applications, *ChemSusChem* 11 (2018) 3546–3558, <https://doi.org/10.1002/cssc.201801525>.
- [25] S. Zheng, L. Miao, T. Sun, L. Li, T. Ma, J. Bao, Z. Tao, J. Chen, An extended carbonyl-rich conjugated polymer cathode for high-capacity lithium-ion batteries, *J. Mater. Chem. A* 9 (2021) 2700–2705, <https://doi.org/10.1039/D0TA11648C>.
- [26] D. Kim, J. Kang, B. Yan, K.D. Seong, Y. Piao, Ambient temperature synthesis of iron-doped porous nickel pyrophosphate nanoparticles with long-term chemical stability for high-performance oxygen evolution reaction catalysis and supercapacitors, *ACS Sustainable Chem. Eng.* 8 (2020) 2843–2853, <https://doi.org/10.1021/acsuschemeng.9b06920>.
- [27] Y. Liao, H. Wang, M. Zhu, A. Thomas, Efficient supercapacitor energy storage using conjugated microporous polymer networks synthesized from buchwald-hartwig coupling, *Adv. Mater.* 30 (2018) 1705710, <https://doi.org/10.1002/adma.201705710>.
- [28] Z. Lin, E. Goikolea, A. Balducci, K. Naoi, P.L. Taberna, M. Salanne, G. Yushin, P. Simon, Materials for supercapacitors: when li-ion battery power is not enough, *Mater. Today* 21 (2018) 419–436, <https://doi.org/10.1016/j.mattod.2018.01.035>.
- [29] Y.G. Wang, Y.F. Song, Y.Y. Xia, Electrochemical capacitors: mechanism, materials, systems, characterization and applications, *Chem. Soc. Rev.* 45 (2016) 5925–5950, <https://doi.org/10.1039/C5CS00580A>.
- [30] J.S. Lee, A.I. Cooper, Advances in conjugated microporous polymers, *Chem. Rev.* 120 (2020) 2171–2214, <https://doi.org/10.1021/acs.chemrev.9b00399>.
- [31] M.G. Mohamed, E.C. Atayde Jr, M.B. Matsagar, J. Na, Y. Yamauchi, K.C.W. Wu, S. W. Kuo, Construction hierarchically mesoporous/microporous materials based on block copolymer and covalent organic framework, *J. Taiwan Inst. Chem. Eng.* 112 (2020) 180–192, <https://doi.org/10.1016/j.jtice.2020.06.013>.
- [32] Y. Zhang, B. Zhang, L. Chen, T. Wang, M. Di, F. Jiang, X. Xu, S. Qiao, Rational design of covalent triazine frameworks based on pore size and heteroatomic toward high performance supercapacitors, *J. Colloid Interface Sci.* 606 (2022) 1534–1542, <https://doi.org/10.1016/j.jcis.2021.08.087>.
- [33] M.G. Mohamed, M.H. Elsayed, A.M. Elewa, A.F.M. EL-Mahdy, C.H. Yang, A.A. K. Mohammed, H.H. Chou, S.W. Kuo, Pyrene-containing conjugated organic microporous polymers for photocatalytic hydrogen evolution from water, *Catal. Sci. Technol.* 11 (2021) 2229–2241, <https://doi.org/10.1039/D0CY02482A>.
- [34] H. Wang, Z. Cheng, Y. Liao, J. Li, J. Weber, A. Thomas, C.F.J. Faul, Conjugated Microporous polycarbazole networks as precursors for nitrogen-enriched microporous carbons for CO₂ storage and electrochemical capacitors, *Chem. Mater.* 29 (2017) 4885–4893, <https://doi.org/10.1021/acs.chemmater.7b00857>.
- [35] V.S. Mothika, M. Baumgarten, U. Scherf, Neutral, π -radical-conjugated microporous polymer films of nanoscale thickness for potential use in magnetoelectronics and sensor devices, *ACS Appl. Nano Mater.* 2 (2019) 4832–4841, <https://doi.org/10.1021/acsanm.9b00776>.
- [36] Z. Weng, Y. Su, D.W. Wang, F. Li, J. Du, H.M. Cheng, Graphene–cellulose paper flexible supercapacitors, *Adv. Energy Mater.* 1 (2011) 917–922, <https://doi.org/10.1002/aenm.201100312>.
- [37] D.H. Roh, H. Shin, H.T. Kim, T.H. Kwon, Sono-cavitation and nebulization-based synthesis of conjugated microporous polymers for energy storage applications, *ACS Appl. Mater. Inter.* 13 (2021) 61598–61609, <https://doi.org/10.1021/acsami.1c13755>.
- [38] X. Jiang, K. Zhang, Y. Huang, B. Xu, X. Xu, J. Zhang, Z. Liu, Y. Wang, Y. Pan, S. Bian, Q. Chen, Conjugated microporous polymer with C≡C and C-F bonds: achieving remarkable stability and super anhydrous proton conductivity, *ACS Appl. Mater. Inter.* 13 (2021) 15536–15541, <https://doi.org/10.1021/acsami.1c02355>.
- [39] M.G. Mohamed, M.Y. Tsai, C.F. Wang, C.F. Huang, M. Danko, L. Dai, T. Chen, S. W. Kuo, Multifunctional polyhedral oligomeric silsesquioxane (POSS) based hybrid porous materials for CO₂ uptake and iodine adsorption, *Polymers* 13 (2021) 221, <https://doi.org/10.3390/polym13020221>.
- [40] X. Lou, J. Chen, Z. Xiong, D. Tang, X. Chen, S. Chen, R. Dong, C. Ye, T. Qiu, Porosity design on conjugated microporous poly(aniline)s for exceptional mercury (II) removal, *ACS Appl. Mater. Inter.* 13 (2021) 61653–61660, <https://doi.org/10.1021/acsami.1c19011>.
- [41] Z. Zhou, X. Li, D. Guo, D.B. Shinde, D. Lu, L. Chen, X. Liu, L. Cao, A.M. Aboalsaud, Y. Hu, Z. Lai, Electropolymerization of robust conjugated microporous polymer membranes for rapid solvent transport and narrow molecular sieving, *Nat. Commun.* 11 (2020) 5323, <https://doi.org/10.1038/s41467-020-19182-1>.
- [42] M.G. Mohamed, S.U. Sharma, N.Y. Liu, T.H. Mansoure, M.M. Samy, S.V. Chaganti, Y.L. Chang, J.T. Lee, S.W. Kuo, Ultrastable covalent triazine organic framework based on anthracene moiety as platform for high-performance carbon dioxide adsorption and supercapacitors, *Int. J. Mol. Sci.* 23 (2022) 3174, <https://doi.org/10.3390/ijms23063174>.
- [43] Z. Liu, Y. Yin, M. Eginligil, L. Wang, J. Liu, W. Huang, Two-dimensional conjugated microporous polymer films: fabrication strategies and potential applications, *Polym. Chem.* 12 (2021) 807–821, <https://doi.org/10.1039/D0PY01368D>.
- [44] M.G. Mohamed, M.M. Samy, T.H. Mansoure, S.U. Sharma, M.S. Tsai, J.H. Chen, J. T. Lee, S.W. Kuo, Dispersions of 1,3,4-Oxadiazole-linked conjugated microporous polymers with carbon nanotubes as a high-performance electrode for supercapacitors, *ACS Appl. Energy Mater.* 5 (2022) 3677–3688, <https://doi.org/10.1021/acsaeam.2c00100>.
- [45] M.M. Samy, I.M.A. Mekhemer, M.G. Mohamed, M.H. Elsayed, K.H. Lin, Y.K. Chen, T.L. Wu, H.H. Chou, S.W. Kuo, Conjugated microporous polymers incorporating Thiazol[5,4-d]thiazole moieties for Sunlight-Driven hydrogen production from water, *Chem. Eng. J.* 446 (2022), 137158, <https://doi.org/10.1016/j.cej.2022.137158>.
- [46] S. Das, P. Heasman, T. Ben, S. Qiu, Porous organic materials: strategic design and structure–function correlation, *Chem. Rev.* 117 (2017) 1515–1563, <https://doi.org/10.1021/acs.chemrev.6b00439>.
- [47] M.G. Mohamed, A.F.M. EL-Mahdy, M.G. Kotp, S.W. Kuo, Advances in porous organic polymers: syntheses, structures, and diverse applications *Mater. Adv.* 3 (2022) 707–733, <https://doi.org/10.1039/D1MA000771H>.
- [48] M.G. Mohamed, T.C. Chen, S.W. Kuo, Solid-state chemical transformations to enhance gas capture in benzoxazine-linked conjugated microporous polymers, *Macromolecules* 54 (2021) 5866–5877, <https://doi.org/10.1021/acs.macromol.1c00736>.

- [49] D. Chen, C. Liu, J. Tang, L. Luo, G. Yu, Fluorescent porous organic polymers, *Polym. Chem.* 10 (2019) 1168–1181, <https://doi.org/10.1039/C8PY01620H>.
- [50] Z. Yan, J. Liu, C. Miao, P. Su, G. Zheng, B. Cui, T. Geng, J. Fan, Z. Yu, N. Bu, Y. Yuan, L. Xia, Pyrene-based fluorescent porous organic polymers for recognition and detection of pesticides, *Molecules* 27 (2022) 126, <https://doi.org/10.3390/molecules27010126>.
- [51] K.Y. Geng, T. He, R.Y. Liu, S. Dalapati, K.T. Tan, Z.P. Li, S.H. Tao, Y.F. Gong, Q. H. Jiang, D.L. Jiang, Covalent organic frameworks: Design, synthesis, and functions, *Chem. Rev.* 16 (2020) 8814–8933, <https://doi.org/10.1021/acs.chemrev.9b00550>.
- [52] S. Kotha, M. Meshram, N.R. Panguluri, V. Shah, S. Todeti, M.E. Shirbhate, Synthetic approaches to star-shaped molecules with 1,3,5-trisubstituted aromatic cores, *Chem. Asian J.* 14 (2019) 1356–1403, <https://doi.org/10.1002/asia.201801912>.
- [53] T. Geng, M. Liu, C. Zhang, C. Hu, H. Xu, Synthesis of secondary amine-based fluorescent porous organic polymers via Friedel-Crafts polymerization reaction for adsorbing and fluorescent sensing iodine, *J. Appl. Polym. Sci.* 13 (2020) 49255, <https://doi.org/10.1002/app.49255>.
- [54] Y. Yuan, H. Ren, F. Sun, X. Jing, K. Cai, X. Zhao, Y. Wang, Y. Wei, G. Zhu, Sensitive detection of hazardous explosives via highly fluorescent crystalline porous aromatic frameworks, *J. Mater. Chem.* 22 (2012) 24558–24562, <https://doi.org/10.1039/C2JM35341E>.
- [55] Z.J. Yan, H. Ren, H.P. Ma, R.R. Yuan, Y. Yuan, X.Q. Zou, F.X. Sun, G.S. Zhu, Construction and sorption properties of pyrene-based porous aromatic frameworks, *Microporous Mesoporous Mater.* 173 (2013) 92–98, <https://doi.org/10.1016/j.micromeso.2013.02.006>.
- [56] S. Wang, H. Li, H. Huang, X. Cao, X. Chen, D. Cao, Porous organic polymers as a platform for sensing applications, *Chem. Soc. Rev.* 51 (2022) 2031–2080, <https://doi.org/10.1039/D2CS00059H>.
- [57] M. Ejaz, M.G. Mohamed, S.U. Sharma, J.T. Lee, C.F. Huang, T. Chen, S.W. Kuo, An ultrastable porous polyhedral oligomeric silsesquioxane/tetraphenylthiophene hybrid as a high-performance electrode for supercapacitors, *Molecules* 27 (2022) 6238, <https://doi.org/10.3390/molecules27196238>.
- [58] M.G. Mohamed, M.M.M. Ahmed, W.T. Du, S.W. Kuo, Meso/microporous carbons from conjugated hyper-crosslinked polymers based on tetraphenylethene for high-performance CO₂ capture and supercapacitor, *Molecules* 26 (2021) 738, <https://doi.org/10.3390/molecules26030738>.
- [59] M.G. Mohamed, T.H. Mansoure, M.M. Samy, Y. Takashi, A.A.K. Mohammed, T. Ahamad, S.M. Alshehri, J. Kim, B.M. Matsagar, K.C.W. Wu, S.W. Kuo, Ultrastable conjugated microporous polymers containing benzobisthiadiazole and pyrene building blocks for energy storage applications, *Molecules* 27 (2022) 2025, <https://doi.org/10.3390/molecules27062025>.
- [60] M.G. Mohamed, W.C. Chang, S.W. Kuo, Crown ether- and benzoxazine-linked porous organic polymers displaying enhanced metal ion and CO₂ capture through solid-state chemical transformation, *Macromolecules* 55 (2022) 7879–7892, <https://doi.org/10.1021/acs.macromol.2c01216>.
- [61] S. Chandrasekar, C. Chandrasekaran, T. Muthukumarasamyvel, G. Sudhandiran, N. Rajendiran, Biosurfactant templated quantum sized fluorescent gold nanoclusters for in vivo bioimaging in zebrafish embryos, *Colloids Surf. B: Biointerfaces* 143 (2016) 472–480, <https://doi.org/10.1016/j.colsurfb.2016.03.067>.
- [62] M. Madhu, T.H. Chen, W.L. Tseng, White-light emission of single carbon dots prepared by hydrothermal carbonization of poly(diallyldimethylammonium chloride): Applications to fabrication of white-light-emitting films, *J. Colloid Interface Sci.* 556 (2019) 120–127, <https://doi.org/10.1016/j.jcis.2019.08.049>.
- [63] M.M.G. Mohamed, H.Y. Hu, M. Madhu, M. Ejaz, S.U. Sharma, W.T. Tseng, M. M. Samy, C.W. Huang, J.T. Lee, S.W. Kuo, Construction of ultrastable conjugated microporous polymers containing thiophene and fluorene for metal ion sensing and energy storage, *Micromachines* 13 (2022) 1466, <https://doi.org/10.3390/mi13091466>.
- [64] M. Madhu, C.M. Chao, C.Y. Ke, M.M. Hsieh, W.L. Tseng, Directed self-assembly of Ag⁺-deposited MoS₂ quantum dots for colorimetric, fluorescent and fluorescence-lifetime sensing of alkaline phosphatase, *Anal Bioanal Chem.* 414 (2022) 1909–1919, <https://doi.org/10.1007/s00216-021-03826-2>.
- [65] M.G. Mohamed, M.M. Samy, T.H. Mansoure, C.J. Li, W.C. Li, J.H. Chen, K. Zhang, S.W. Kuo, Microporous carbon and carbon/metal composite materials derived from bio-benzoxazine-linked precursor for CO₂ capture and energy storage applications, *Int. J. Mol. Sci.* 23 (2022) 347, <https://doi.org/10.3390/ijms23010347>.
- [66] Y. Li, S. Zheng, X. Liu, P. Li, L. Sun, R. Yang, S. Wang, Z.S. Wu, X. Bao, W.Q. Deng, Conductive microporous covalent triazine-based framework for high-performance electrochemical capacitive energy storage, *Angew. Chem. Int. Ed.* 130 (2018) 8124–8128, <https://doi.org/10.1002/ange.201711169>.
- [67] F. Hu, J. Wang, S. Hu, L. Li, W. Shao, J. Qiu, Z. Lei, W. Deng, X. Jian, Engineered fabrication of hierarchical frameworks with tuned pore structure and N, O-codoping for high-performance supercapacitors, *ACS Appl. Mater. Inter.* 37 (2017) 31940–31949, <https://doi.org/10.1021/acsami.7b09801>.
- [68] A.M. Khattak, Z.A. Ghazi, B. Liang, N.A. Khan, A. Iqbal, L. Li, Z. Tang, A redox-active 2D covalent organic framework with pyridine moieties capable of faradaic energy storage, *J. Mater. Chem. A.* 4 (2016) 16312–16317, <https://doi.org/10.1039/C6TA05784E>.